

# Thermal expansivity of geikielite and ilmenite utilizing in-situ synchrotron X-ray diffraction at high temperature

Jiamei Song<sup>1,2</sup> · Dawei Fan<sup>1</sup> · Shijie Huang<sup>1,2</sup> · Shanrong Zhang<sup>1,2</sup> ·  
Mengzeng Wu<sup>1,2</sup> · Wei Chen<sup>1,2,3</sup> · Wenge Zhou<sup>1</sup>

Received: 31 March 2023 / Revised: 12 July 2023 / Accepted: 24 July 2023 / Published online: 19 August 2023  
© The Author(s), under exclusive licence to Science Press and Institute of Geochemistry, CAS and Springer-Verlag GmbH Germany, part of Springer Nature 2023

**Abstract** The unit-cell parameters and volumes of geikielite ( $\text{MgTiO}_3$ ) and ilmenite ( $\text{FeTiO}_3$ ) were investigated at high temperatures up to 700 K and ambient pressure, using in-situ angle-dispersive synchrotron X-ray diffraction. No phase transition was detected over the experimental temperature range. Using (Berman in *J Petrol* 29:445–522, 1988. 10.1093/petrology/29.2.445) equations to fit the temperature-volume data, the volumetric thermal expansion coefficients at ambient conditions ( $\alpha_{V0}$ ) of  $\text{MgTiO}_3$  and  $\text{FeTiO}_3$  were obtained as follows:  $2.55(6) \times 10^{-5} \text{ K}^{-1}$  and  $2.82(10) \times 10^{-5} \text{ K}^{-1}$ , respectively. We infer that the larger effective ionic radius of  $\text{Fe}^{2+}$ (VI) (0.78 Å) than that of  $\text{Mg}^{2+}$ (VI) (0.72 Å) renders  $\text{FeTiO}_3$  has a larger volumetric thermal expansivity than  $\text{MgTiO}_3$ . Simultaneously, the refined axial thermal expansion coefficients under ambient conditions are  $\alpha_{a0} = 0.74(3) \times 10^{-5} \text{ K}^{-1}$  and  $\alpha_{c0} = 1.08(5) \times 10^{-5} \text{ K}^{-1}$  for the  $a$ -axis and  $c$ -axis of  $\text{MgTiO}_3$ , respectively, and  $\alpha_{a0} = 0.95(5) \times 10^{-5} \text{ K}^{-1}$  and  $\alpha_{c0} = 0.92(12) \times 10^{-5} \text{ K}^{-1}$  for the  $a$ -axis and  $c$ -axis of  $\text{FeTiO}_3$ , respectively. The axial thermal expansivity of  $\text{MgTiO}_3$  is anisotropic, but that of  $\text{FeTiO}_3$  is nearly isotropic. We infer that the main reason for the different axial thermal expansivity between  $\text{MgTiO}_3$  and

$\text{FeTiO}_3$  is that the thermal expansion mode of the Mg–O bond in  $\text{MgTiO}_3$  is different from that of the Fe–O bonds in  $\text{FeTiO}_3$ .

**Keywords** Geikielite · Ilmenite · Thermal expansion · Synchrotron X-ray diffraction · High temperature

## 1 Introduction

The lunar interior is thought to consist of various mineral accumulations resulting from the crystallization differentiation of early magmatic oceans (Wieczorek et al. 2006). At the end stage of the early lunar evolution, the ilmenite-bearing cumulates (IBCs) layer, which is composed mainly of ilmenite ( $\text{FeTiO}_3$ ), is formed in the upper lunar mantle, and then overturned and sunk to the deep lower lunar mantle (Zhao et al. 2019). The downwelling of IBCs after lunar mantle overturning has an important impact on the dynamics and thermal evolution of the lunar mantle (Xu 2010). The density characteristics of IBCs, especially the density of  $\text{FeTiO}_3$  at the corresponding pressure and temperature conditions, are one of the key parameters to gain insight into the dynamics process of lunar mantle overturning (Li et al. 2019).

The density characteristics of  $\text{FeTiO}_3$  require the thermodynamic parameters of  $\text{FeTiO}_3$  under the corresponding high pressure and temperature conditions. Among them, the thermal expansion coefficient is an important thermodynamic parameter for constructing the density model of  $\text{FeTiO}_3$  under the corresponding high pressure and temperature conditions. Thus, the study of the thermal expansion coefficient of  $\text{FeTiO}_3$  is fundamental for constructing the density model of lunar mantle under the

✉ Dawei Fan  
fandawei@vip.gyig.ac.cn

<sup>1</sup> Key Laboratory of High-Temperature and High-Pressure Study of the Earth's Interior, Institute of Geochemistry, Chinese Academy of Sciences, Guiyang 550081, Guizhou, China

<sup>2</sup> University of Chinese Academy of Sciences, Beijing 100049, China

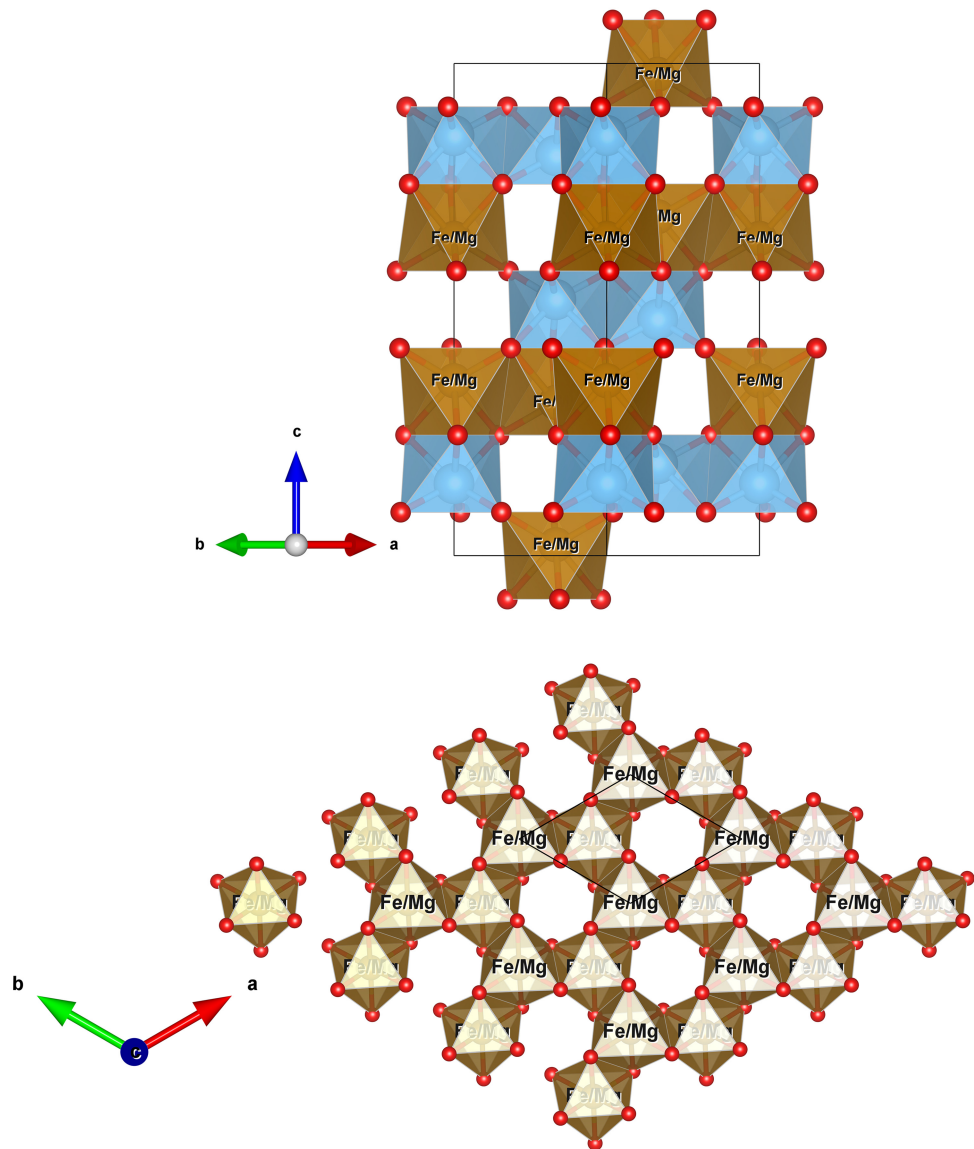
<sup>3</sup> Guizhou Polytechnic of Construction, Guiyang 551400, Guizhou, China

corresponding high pressure and temperature conditions, and then understanding the density characteristics of IBCs and the dynamic process of the lunar mantle overturning.

Previous studies have shown that  $\text{FeTiO}_3$  and geikielite ( $\text{MgTiO}_3$ ) can form unlimited solid solution (Lindsley 1991; Linton et al. 1999) along with crystallization and differentiation of lunar magmatic ocean. In addition, according to the existing detailed mineral composition analysis of Apollo samples, Luna samples, and lunar meteorites, the lunar ilmenite always contains a certain percentage of geikielite. Specifically, the typical content of geikielite in the lunar ilmenite sample is  $\sim 5$  vol%, and the maximum is up to  $\sim 33$  vol% (Alexander et al. 2014, 2016; Anand et al. 2003; Donohue and Neal 2018; Heiken et al. 1991; Hu 2015; Joy et al. 2008; Klemme et al. 2006; Shearer et al. 1991; Snape et al. 2014).

**Fig. 1** Crystal structure (vertical and side views) of  $\text{FeTiO}_3$  and  $\text{MgTiO}_3$  at ambient conditions ( $R\bar{3}$ ). The crystal structure data are obtained from Yamanaka et al. (2005, 2007)

Both  $\text{FeTiO}_3$  and  $\text{MgTiO}_3$  are  $\text{ABO}_3$ -type oxides, which belong to the trigonal system with space group  $R$  (Fig. 1).  $\text{Mg}^{2+}$  can completely replace  $\text{Fe}^{2+}$  at the A cation of  $\text{FeTiO}_3$  to form  $\text{MgTiO}_3$ . In addition, both  $\text{FeTiO}_3$  and  $\text{MgTiO}_3$  consist of  $\text{AO}_6$  ( $\text{A} = \text{Mg, Fe}$ ),  $\text{BO}_6$  ( $\text{B} = \text{Ti}$ ), and  $\text{VO}_6$  (vacancy, which means lacking central ion). A and B cations occupy two-thirds of the octahedral sites in an orderly manner, and  $\text{AO}_6$  and  $\text{BO}_6$  octahedrons have an equal number of divalent ( $\text{A}^{2+}$ ) and tetravalent ( $\text{B}^{4+}$ ) cations, forming alternate layers along the hexagon  $c$  direction, and one-third of the octahedral sites are vacant.  $\text{XO}_6$  ( $\text{X} = \text{A, B}$ ) forms a hexagonal ring centered on  $\text{VO}_6$  and extends within the same layer, and then the  $\text{AO}_6$  and  $\text{BO}_6$  layers are interleaved alternately. The ratio of  $\text{AO}_6$ ,  $\text{BO}_6$ , and  $\text{VO}_6$  is 1:1:1 within the same layer. Along the  $a$ -axis, a pair of shared side  $\text{BO}_6$  octahedrons is separated by



cationic vacancies and diagonally by an  $\text{AO}_6$  octahedron. Along the  $c$ -axis, the cells are arranged in the order of  $\text{AO}_6\text{--BO}_6\text{--VO}_6\text{--BO}_6\text{--AO}_6\text{--VO}_6$ .

To date, only a few previous studies conducted the thermal expansion behavior of  $\text{FeTiO}_3$  and  $\text{MgTiO}_3$  at high temperatures using various experimental methods. For  $\text{FeTiO}_3$ , Wechsler and Prewitt (1984) first researched the high-temperature thermal expansion behavior of  $\text{FeTiO}_3$  from 297 to 1323 K using the conventional single-crystal X-ray diffraction method. Hereafter, Harrison et al. (2000) studied the thermal expansivity of  $\text{FeTiO}_3$  from 293 to 1598 K using the in-situ neutron powder diffraction method. However, there was a significant difference in the thermal expansion coefficients between Wechsler and Prewitt (1984) and Harrison et al. (2000). For  $\text{MgTiO}_3$ , Henderson et al. (2009) first investigated the thermal expansivity of  $\text{MgTiO}_3$  at high temperatures from 296 to 1305 K using in-situ neutron powder diffraction method. Subsequently, Tuval et al. (2020) also measured the thermal expansivity of  $\text{MgTiO}_3$  from 298 to 1163 K using the conventional powder X-ray diffraction method. However, both the experimental samples of Henderson et al. (2009) and Tuval et al. (2020) contain non-negligible impurities, and there is also a big difference in the calculated thermal expansion coefficients between Henderson et al. (2009) and Tuval et al. (2020). Therefore, there are still many deficiencies at present in understanding the thermal expansion behavior of  $\text{FeTiO}_3$  and  $\text{MgTiO}_3$ , and further systematic studies are needed.

In this study, we investigated the thermal expansion behaviors of  $\text{MgTiO}_3$  and  $\text{FeTiO}_3$  at high temperatures up to 700 K by in-situ synchrotron radiation X-ray diffraction (XRD) combined with diamond anvil cell (DAC). Moreover, the potential influencing factors on the volumetric thermal expansivity of  $\text{MgTiO}_3$  and  $\text{FeTiO}_3$  and the different axial thermal expansivities between  $\text{MgTiO}_3$  and  $\text{FeTiO}_3$  were further discussed.

## 2 Samples and analytical methods

The  $\text{MgTiO}_3$  and  $\text{FeTiO}_3$  samples in this study are high-purity (> 99%) powders procured by Aladdin Corporation. The samples were heated for two hours at a constant temperature of 100 °C in a furnace to remove the absorbed moisture and then examined via conventional powder XRD using an Empyrean X-ray diffractometer (DY1411). The cermet X-ray tube (Cu target) has a maximum powder wavelength of 1.5406 Å, a voltage of 40 kV, an operating current of 40 mA, and a range of 5.0051–70°. The ambient XRD spectra of  $\text{MgTiO}_3$  and  $\text{FeTiO}_3$  were indexed based on the standard spectra JCPDS 79-0831 and JCPDS 75-1203, respectively, confirming that the crystal structures

of  $\text{MgTiO}_3$  and  $\text{FeTiO}_3$  are trigonal and belong to the  $R$  space group.

High temperature and ambient pressure experiments were carried out by using a modified Merrill-Bassett type DAC (Fan et al. 2010, 2014) mounted with two pairs of 400 µm culet-sized diamond anvils. For the  $\text{MgTiO}_3$  sample, a gasket made of rhenium tablet was preindented to ~ 54 µm thick, and then a ~ 220 µm hole was drilled as the sample chamber. Similarly, for the  $\text{FeTiO}_3$  sample, a gasket made from T301 stainless steel was pre-indented to a thickness of ~ 75 µm and then drilled to a diameter of ~ 230 µm, serving as the sample chamber. The  $\text{FeTiO}_3$  and  $\text{MgTiO}_3$  sample powders were slightly pressed between two opposing diamond anvils to form an approximately 50 µm thick disk, and a piece of  $\text{FeTiO}_3$  or  $\text{MgTiO}_3$  sample about 200 µm in diameter was loaded into the sample chamber. The high temperature was generated by an external resistance heating device made up of a 0.3 mm diametric NiCr resistor wire. Using a Pt<sub>90</sub>Rh<sub>10</sub>–Pt<sub>100</sub> thermocouple adhered to a diamond anvil pavilion, the accuracy of measuring the experimental temperature is ± 1 K. The temperature was increased from room temperature to the maximum temperature of 700 K with an interval of 50 K, while the heating was kept for 300 s before the collection of the powder diffraction spectrum. In addition, the typical exposure time for collecting diffraction patterns of the sample is 300 s. Additional details about the experimental device and DAC components can be found in Fan et al. (2010).

In-situ high-temperature synchrotron radiation angle-dispersive XRD (ADXRD) experiments were conducted at the 4W2 beam-line of the Beijing Synchrotron Radiation Facility (BSRF). The wavelength of the monochromatic X-ray beam is 0.6199 Å calibrated by scanning through the Mo metal  $K$ -absorption edge. Diffraction patterns were amassed using the Pilatus detector. The X-ray beam was collimated to a beam dimension of 20 × 30 µm<sup>2</sup> through a pair of Kirkpatrick-Baez mirrors.  $\text{CeO}_2$  powder was used as the standard for XRD to calibrate the tilting and rotation of the detector to the incident X-ray beam. The sample-detector distance was calculated from the powder  $\text{CeO}_2$  diffraction pattern at ambient conditions.

All collected diffraction patterns were integrated in terms of  $2\theta$  using the Fit2D program to obtain conventional one-dimensional profiles (Hammersley et al. 1996). The unit-cell parameters and volumes were calculated according to the 11 and 14 diffraction peaks identified from the XRD patterns of  $\text{MgTiO}_3$  and  $\text{FeTiO}_3$ , respectively (Fig. 2). Then the diffraction peak positions were fitted using the OriginPro 8.5 software, and the unit-cell parameters and volumes were calculated using UnitCell software (Holland and Redfern 1997). Finally, the

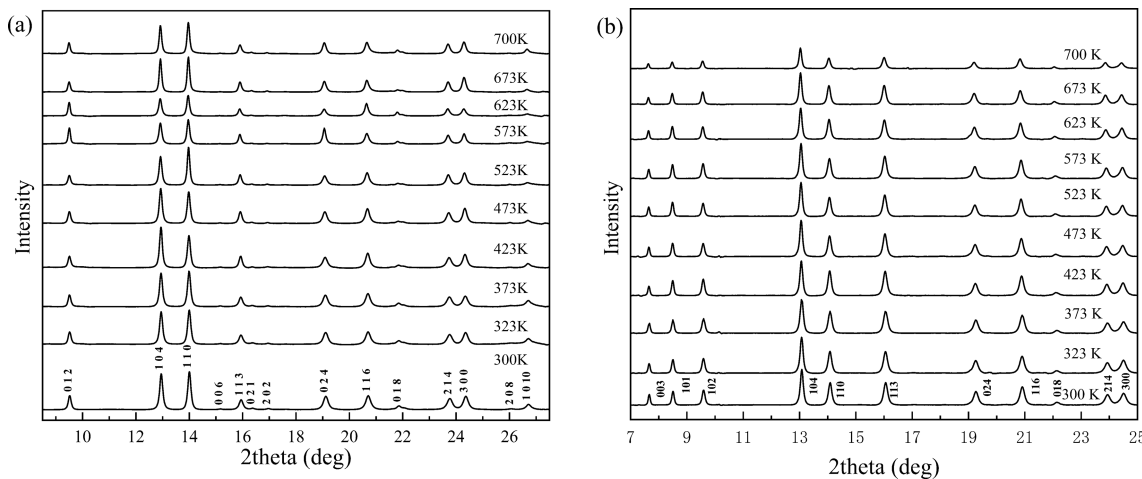


**Fig. 2** Representative X-ray diffraction patterns of  $\text{FeTiO}_3$  (a) and  $\text{MgTiO}_3$  (b) obtained in this study up to 700 K at ambient pressure

volumetric and axial thermal expansion coefficients were fitted using *EoSFit 7* software (Angel et al. 2014).

### 3 Results

The ambient XRD images of  $\text{MgTiO}_3$  and  $\text{FeTiO}_3$  in this study were also obtained at the 4W2 beam-line of BSRF, and the unit-cell parameters and volumes at ambient conditions are shown as follows:  $a_0 = 5.0592(7)$  Å,  $c_0 = 13.889(3)$  Å, and  $V_0 = 307.87(8)$  Å<sup>3</sup> for  $\text{MgTiO}_3$  and  $a_0 = 5.0871(7)$  Å,  $c_0 = 14.070(5)$  Å, and  $V_0 = 315.33(10)$  Å<sup>3</sup> for  $\text{FeTiO}_3$ . Since the ionic radius of  $\text{Mg}^{2+}$  is smaller than that of  $\text{Fe}^{2+}$ , the formed  $\text{Mg}^{2+}\text{-O}$  bond is shorter than the  $\text{Fe}^{2+}\text{-O}$  bond (Henderson et al. 2009; Lifervich and Mitchell 2006; Wechsler and Prewitt 1984; Wechsler and Von Dreele 1989; Yamanaka et al. 2005), and all of the unit-cell parameters and volumes of the  $\text{MgTiO}_3$  sample at ambient conditions are smaller than those of the  $\text{FeTiO}_3$  sample.

The evolution of the XRD patterns of  $\text{MgTiO}_3$  and  $\text{FeTiO}_3$  in the experimental temperature range are shown in Fig. 2, where all peaks shift toward lower  $2\theta$  angles as the temperatures increase from 300 to 700 K at ambient pressure. The characteristic of the XRD patterns of  $\text{MgTiO}_3$  and  $\text{FeTiO}_3$  samples is that the narrow peaks are independent of each other (Fig. 2), which means that the data have high reliability. No peaks disappeared or new peaks appeared within the experimental temperature range, indicating that both  $\text{MgTiO}_3$  and  $\text{FeTiO}_3$  are stable within the experimental temperature conditions in this study. The unit-cell parameters and volumes of  $\text{MgTiO}_3$  and  $\text{FeTiO}_3$  at various temperature conditions are listed in Tables 1 and 2, respectively. Moreover, when the experimental temperature reaches 673 K, the unit-cell parameters and volume of  $\text{FeTiO}_3$  suddenly decrease. However, previous studies

**Table 1** Unit-cell parameters in  $\text{MgTiO}_3$  at high temperature and ambient pressure

T (K)	$a$ (Å)	$c$ (Å)	$V$ (Å <sup>3</sup> )	$c/a$
300	5.0592 (7)	13.889 (3)	307.87 (8)	2.7453
323	5.0601(7)	13.895 (3)	308.11 (8)	2.7460
373	5.0620 (7)	13.899 (3)	308.43 (8)	2.7458
423	5.0636 (7)	13.906 (3)	308.79 (8)	2.7463
473	5.0654 (7)	13.916 (3)	309.24 (8)	2.7473
523	5.0674 (7)	13.922 (3)	309.59 (8)	2.7474
573	5.0690 (7)	13.931 (3)	309.99 (8)	2.7483
623	5.0714 (7)	13.938 (3)	310.44 (8)	2.7484
673	5.0732 (7)	13.945 (3)	310.82 (8)	2.7488
700	5.0740 (7)	13.949 (3)	311.01 (8)	2.7491

Numbers in parenthesis represent standard deviations

**Table 2** Unit-cell parameters in  $\text{FeTiO}_3$  at high temperature and ambient pressure

T (K)	$a$ (Å)	$c$ (Å)	$V$ (Å <sup>3</sup> )	$c/a$
300	5.0871 (7)	14.070 (5)	315.33 (10)	2.76582
323	5.0885 (7)	14.074 (5)	315.60 (10)	2.76584
373	5.0908 (7)	14.078 (5)	315.97 (10)	2.76538
423	5.0933 (7)	14.082 (5)	316.37 (10)	2.76481
473	5.0953 (8)	14.091 (5)	316.82 (10)	2.76549
523	5.0979 (8)	14.098 (5)	317.31 (10)	2.76545
573	5.1005 (8)	14.105 (5)	317.78 (10)	2.76542
623	5.1028 (8)	14.112 (5)	318.23 (10)	2.76554
673	5.1006 (8)	14.099 (5)	317.64 (10)	2.76418
700	5.1012 (8)	14.097 (5)	317.69 (10)	2.76347

Numbers in parenthesis represent standard deviations

(Wechsler and Prewitt 1984; Harrison et al. 2000) have not shown the same phenomenon at higher temperatures. We consider that the main reason for this difference is that the previous high-temperature measurements were carried out under the conditions of controlling the oxygen fugacity of the sample chamber. Such as, Wechsler and Prewitt (1984) studied only one quadrant of reciprocal space to minimize the total exposure of sample chamber at high temperatures. In addition, Harrison et al. (2000) even used a more stringent means of anti-oxidation, i.e. FeTiO<sub>3</sub> was placed in a vacuum furnace for high temperature experiments. Thus, we infer that the oxidation (or partial oxidation) of Fe<sup>2+</sup> (0.780 Å) to Fe<sup>3+</sup> (0.645 Å) in FeTiO<sub>3</sub> caused the sudden drop of the unit-cell parameters and volumes of FeTiO<sub>3</sub> at 673 K. Certainly, further experiments (e.g. recovering the experimental samples for Mössbauer spectroscopy measurement) are needed to confirm whether Fe<sup>2+</sup> oxidation occurs at 673 K.

The temperature-volume (*T*-*V*) statistics (Tables 1 and 2, Fig. 3) were used to fit the volumetric thermal expansion coefficients of MgTiO<sub>3</sub> and FeTiO<sub>3</sub> at temperatures up to 700 K and 623 K, respectively. In this study, the high-temperature data are fitted with the thermal expansion expression proposed by Berman (1988), and the formula is as follows:

$$V_T = V_0 \times (1 + \alpha_0 \times (T - T_{ref}) + \frac{1}{2} \times \alpha_1 \times (T - T_{ref})^2) \quad (1)$$

where  $V_T$  is the unit-cell volume at elevated temperatures and ambient pressure,  $V_0$  represents the unit-cell volume under ambient conditions, and  $T_{ref}$  is the reference temperature. The relationship between the thermal expansion coefficient and temperature is expressed by the parameters

$\alpha_0$  and  $\alpha_1$  as follows:  $\alpha \approx [\alpha_0 + \alpha_1(T - T_{ref})]$ . The parameter  $\alpha_0$  is the thermal expansion coefficient at  $T_{ref}$ . Figure 3 shows the volumetric thermal expansivities of MgTiO<sub>3</sub> and FeTiO<sub>3</sub> as a function of the temperature in this study. For comparison, the results of Henderson et al. (2009), Tuval et al. (2020), Wechsler and Prewitt (1984), and Harrison et al. (2000) are also plotted on these figures. By fitting the Eq. (1) based on the unit-cell volumes in this study with the *EoSFit* 7 program, we obtained the volumetric thermal expansion coefficients at ambient conditions  $\alpha_{V0} = 2.55 (6) \times 10^{-5} \text{ K}^{-1}$  for MgTiO<sub>3</sub> and  $\alpha_{V0} = 2.82 (10) \times 10^{-5} \text{ K}^{-1}$  for FeTiO<sub>3</sub> (Two data points with temperatures above 623 K were not used for fitting).

Figures 4 and 5 show the axial thermal expansivities of MgTiO<sub>3</sub> and FeTiO<sub>3</sub> as a function of temperature. By fitting the unit-cell parameter data ( $a$  and  $c$ ) of MgTiO<sub>3</sub> and FeTiO<sub>3</sub> at high temperatures up to 700 K and 623 K using a “linearized” Berman’s equation  $l_T = l_0 \times (1 + \alpha_0 \times (T - T_{ref}))$  ( $l = a, b, c$ ) with the *EoSFit* 7 program (Angel et al. 2014; Gonzalez-Platas et al. 2016), the refined unit-cell parameters at ambient conditions were obtained as follows:  $a_0 = 5.0591(4) \text{ \AA}$  and  $c_0 = 13.889(2) \text{ \AA}$  for MgTiO<sub>3</sub> and  $a_0 = 5.0871(4) \text{ \AA}$  and  $c_0 = 14.069(3) \text{ \AA}$  for FeTiO<sub>3</sub>. The refined unit-cell parameters at ambient conditions are consistent with the measured results at ambient conditions in this study within their uncertainties (Tables 1 and 2). Simultaneously, the refined axial thermal expansion coefficients under ambient conditions are  $\alpha_{a0} = 0.74 (3) \times 10^{-5} \text{ K}^{-1}$  and  $\alpha_{c0} = 1.08 (5) \times 10^{-5} \text{ K}^{-1}$  for MgTiO<sub>3</sub> and  $\alpha_{a0} = 0.95 (5) \times 10^{-5} \text{ K}^{-1}$  and  $\alpha_{c0} = 0.92 (12) \times 10^{-5} \text{ K}^{-1}$  for FeTiO<sub>3</sub> (Two data points with temperatures above 623 K were not used for fitting).

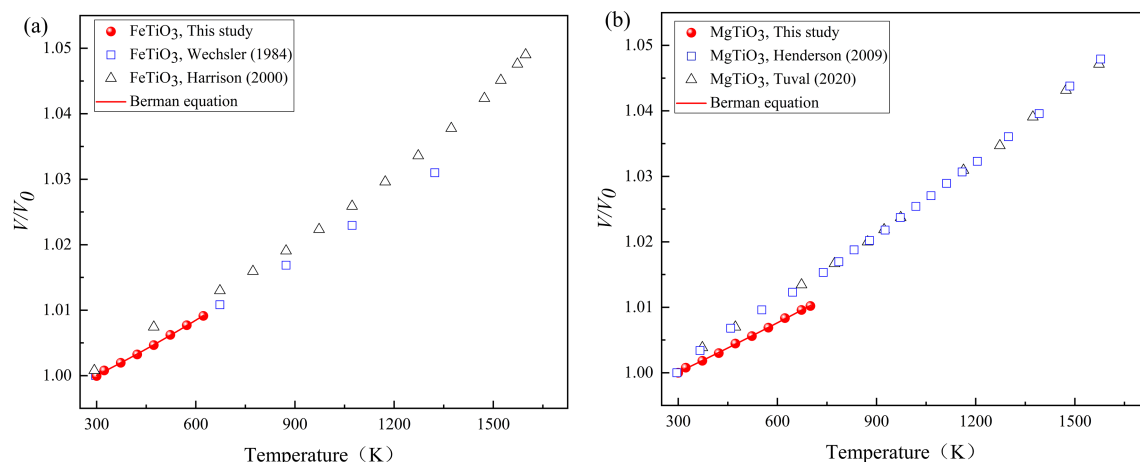


**Fig. 3** *T*-*V* data of FeTiO<sub>3</sub> (a) and MgTiO<sub>3</sub> (b) at ambient pressure ((Harrison et al. 2000; Henderson et al. 2009; Tuval et al. 2020; Wechsler and Prewitt 1984). The error bars for the data points are not displayed because they are smaller than the symbols

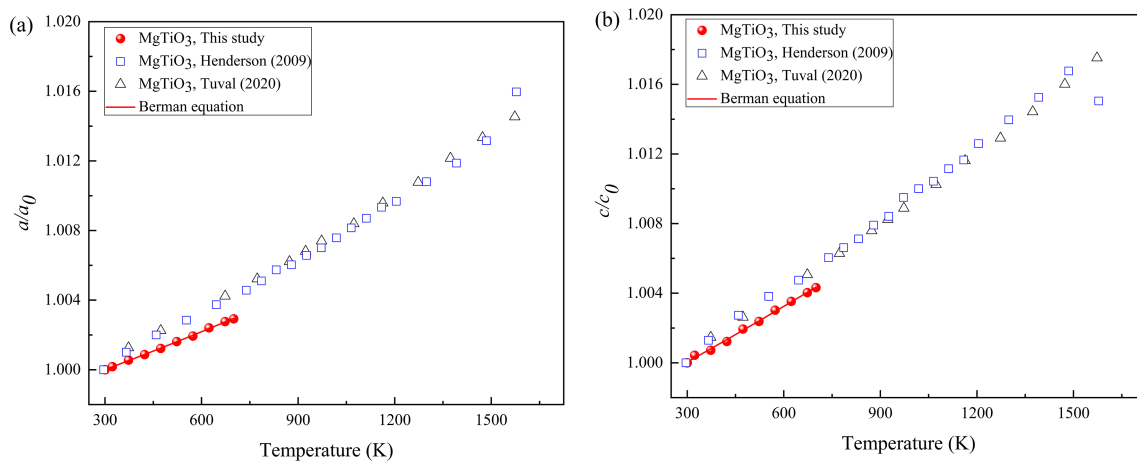


**Fig. 4** Temperature dependence of the unit-cell parameters  $a$  and  $c$  of  $\text{MgTiO}_3$  at room pressure (Henderson et al. 2009; Tuval et al. 2020)

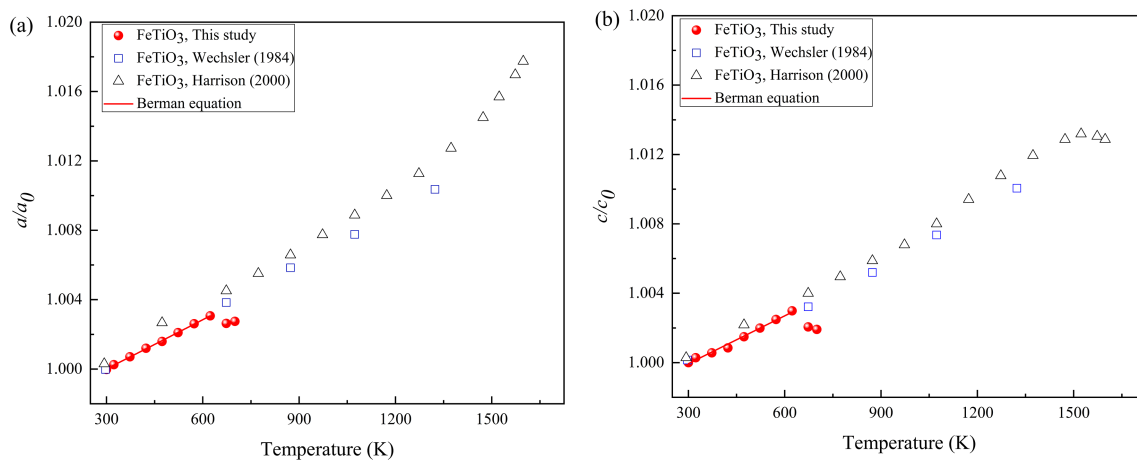


**Fig. 5** Temperature dependence of the unit-cell parameters  $a$  and  $c$  of  $\text{FeTiO}_3$  at room pressure (Harrison et al. 2000; Wechsler and Prewitt 1984)

#### 4 Discussion

The thermal expansion coefficients of  $\text{MgTiO}_3$  and  $\text{FeTiO}_3$  have been investigated by some previous studies. Table 3 shows a detailed comparison between the thermal expansion coefficients of  $\text{FeTiO}_3$  and  $\text{MgTiO}_3$  obtained in this study and previous studies.

For  $\text{FeTiO}_3$ , only Wechsler and Prewitt (1984) and Harrison et al. (2000) investigated the temperature dependence of the unit-cell parameters and volumes of  $\text{FeTiO}_3$  at high temperatures, but they have not given the volumetric and axial thermal expansion coefficients of  $\text{FeTiO}_3$ . Thus, we recalculated the volumetric and axial thermal expansion coefficients of  $\text{FeTiO}_3$  by fitting their unit-cell parameters and volumes of  $\text{FeTiO}_3$  at high temperatures using Berman's equation (Berman 1988), and the results are shown in Table 3 and Fig. 5 (Two data points with temperatures above 1500 K were not used for fitting). From Table 3, we can find that the values of volumetric thermal expansion

coefficient of  $\text{FeTiO}_3$  at ambient conditions from this study and previous studies are within the range of  $(2.82\text{--}3.62) \times 10^{-5} \text{ K}^{-1}$ . In this study, the obtained  $\alpha_{V0} = 2.82 (10) \times 10^{-5} \text{ K}^{-1}$  for  $\text{FeTiO}_3$  is roughly similar to the  $\alpha_{V0} = 3.02 (4) \times 10^{-5} \text{ K}^{-1}$  obtained by Wechsler and Prewitt (1984) within their uncertainties. However, both of them are  $\sim 17\text{--}22\%$  lower than the  $\alpha_{V0} = 3.62 (10) \times 10^{-5} \text{ K}^{-1}$  obtained by Harrison et al. (2000). However, the exact reasons for the reported  $\alpha_{V0}$  of Harrison et al. (2000) larger than those of this study and Wechsler and Prewitt (1984) are still unknown.

For  $\text{MgTiO}_3$ , Henderson et al. (2009) and Tuval et al. (2020) investigated the thermal expansion behavior of  $\text{MgTiO}_3$  at high temperatures. For the convenience of comparison, their thermal expansion coefficients were obtained by fitting the Berman equation (Table 3). From Table 3, we can find that the values of volumetric thermal expansion coefficient of  $\text{MgTiO}_3$  at ambient conditions from this study and previous studies are within the range of

**Table 3** The refined unit-cell parameters and volumes, and thermal expansion coefficients of MgTiO<sub>3</sub> and FeTiO<sub>3</sub> at ambient conditions by using Berman's equations

	$l_0(\text{\AA}^3)/V(\text{\AA}^3)$	Alpha ( $\times 10^{-5} \text{ K}^{-1}$ )	References
MgTiO <sub>3</sub>			
<i>a</i>	5.0591 (4)	0.74 (3)	
<i>c</i>	13.889 (2)	1.08 (5)	This study
<i>V</i>	307.85 (5)	2.55 (6)	
<i>a</i>	5.0557 (4)	0.94 (3)	
<i>c</i>	13.901 (2)	1.25 (5)	Henderson et al. (2009)
<i>V</i>	307.69 (7)	3.12 (9)	
<i>a</i>	5.0535 (2)	0.845 (5)	
<i>c</i>	13.902 (1)	1.094 (6)	Tuval et al. (2020)
<i>V</i>	307.46 (3)	2.78 (1)	
FeTiO <sub>3</sub>			
<i>a</i>	5.0871 (4)	0.95 (5)	
<i>c</i>	14.069 (3)	0.92 (12)	This study
<i>V</i>	315.31 (6)	2.82 (10)	
<i>a</i>	5.0885 (2)	1.02 (1)	
<i>c</i>	14.083 (3)	0.96 (3)	Wechsler and Prewitt (1984)
<i>V</i>	315.76 (8)	3.02 (4)	
<i>a</i>	5.0865 (17)	1.23 (5)	
<i>c</i>	14.088 (2)	1.05 (2)	Harrison et al. (2000)
<i>V</i>	315.56 (28)	3.62 (10)	

Numbers in parenthesis represent standard deviations

$(2.55\text{--}3.12) \times 10^{-5} \text{ K}^{-1}$ . The obtained  $\alpha_{VO} = 2.55 (6) \times 10^{-5} \text{ K}^{-1}$  for MgTiO<sub>3</sub> in this study is  $\sim 8\%$  and  $\sim 18\%$  lower than the  $\alpha_{VO} = 2.78 (1) \times 10^{-5} \text{ K}^{-1}$  and  $3.12 (9) \times 10^{-5} \text{ K}^{-1}$  obtained by Tuval et al. (2020) and Henderson et al. (2009), respectively. By carefully observing the composition characteristics of MgTiO<sub>3</sub> samples from Tuval et al. (2020) and Henderson et al. (2009), we can find that their MgTiO<sub>3</sub> samples are impure and contain a certain amount of impurities. For example, the MgTiO<sub>3</sub> sample used in Tuval et al. (2020) contains  $\sim 5\%$  Mg<sub>2</sub>TiO<sub>4</sub> (qandilite), and the experimental sample used in Henderson et al. (2009) is MgTi<sub>2</sub>O<sub>5</sub> which is the mixture of geikielite (MgTiO<sub>3</sub>) and rutile (TiO<sub>2</sub>). When samples have other impurity phases, the XRD peaks of samples may overlap with the diffraction signal of the impurity component, which will affect the accuracy of refined unit-cell parameters and volumes of samples. Thus, we infer that the impurities in the MgTiO<sub>3</sub> samples of previous studies may affect their volumetric thermal expansion coefficients of MgTiO<sub>3</sub>.

In summary, the thermal expansion coefficients reported in this study are more reliable compared to those reported in previous studies because of the higher accuracy of the synchrotron XRD method and the higher purity of the samples of FeTiO<sub>3</sub> and MgTiO<sub>3</sub> used in this study. Furthermore, this study also has more experimental points in

the temperature range of 300–700 K, and FeTiO<sub>3</sub> and MgTiO<sub>3</sub> samples were studied under the same experimental system to effectively avoid systematic errors between different experimental systems. All of the above-mentioned factors will result in smaller errors and higher accuracy of unit-cell parameters and volumes, and then obtain more reliable thermal expansion coefficients. Therefore, the influence of components of FeTiO<sub>3</sub> and MgTiO<sub>3</sub> on their volumetric and axial thermal expansion coefficients will be discussed next based on the obtained results in this study.

From Table 3, we can find that the obtained  $\alpha_{VO}$  of FeTiO<sub>3</sub> in this study is  $\sim 10.6\%$  larger than that of MgTiO<sub>3</sub> in this study. As we know, both the Mg and Fe ions occupy the A site in the MgTiO<sub>3</sub> and FeTiO<sub>3</sub>, and the crystal structure difference between MgTiO<sub>3</sub> and FeTiO<sub>3</sub> mainly lies in the change of metal cation types at the A site. The effective ionic radius of Fe<sup>2+</sup>(VI) (0.78 Å) is larger than that of Mg<sup>2+</sup>(VI) (0.72 Å) (Shannon 1976) at A site, which results in that the average bond length of Fe<sup>2+</sup>-O (2.1406 Å) in FeTiO<sub>3</sub> (Yamanaka et al. 2007) is larger than that of Mg<sup>2+</sup>-O (2.10785 Å) in MgTiO<sub>3</sub> (Culbertson et al. 2020). Therefore, the bond strengths of Fe<sup>2+</sup>-O at A site in FeTiO<sub>3</sub> are weaker than that of the Mg<sup>2+</sup>-O at A site in MgTiO<sub>3</sub> due to the larger bond length; accordingly, FeTiO<sub>3</sub> has larger volumetric thermal expansivity than MgTiO<sub>3</sub>.

$\text{MgTiO}_3$  in this study shows the thermal expansion behavior of the  $c$ -axis direction is larger than that of the  $a$ -axis direction. This indicates that  $\text{MgTiO}_3$  is anisotropic axial thermal expansivity (Fig. 6). However,  $\text{FeTiO}_3$  in this study shows the thermal expansion behavior of the  $c$ -axis direction is close to that of the  $a$ -axis direction. This indicates that  $\text{FeTiO}_3$  is quasi-isotropic axial thermal expansivity (Fig. 6). What causes such huge differences in the axial thermal expansion behaviors between  $\text{FeTiO}_3$  and  $\text{MgTiO}_3$ ? Next, we will try to discuss the possible reasons.

From the crystal structure of ilmenite-type minerals, ilmenite has a honeycomb structure along the  $ab$  plane and alternating layers along the  $c$  direction (Fig. 1). The thermal expansion along the  $ab$  plane at high temperatures is determined by the mutual constraint in each plane, and the thermal expansion along  $c$  direction is the average of each layer based on mutual superposition. Moreover, the thermal expansion along the  $ab$  plane and  $c$  direction are mutually constrained. For  $\text{MgTiO}_3$ , the cells tend to expand more along the  $c$ -axis than the  $a$ -axis because the interlayer forces are small, and it is difficult to elongate or bend the  $\text{Mg}–\text{O}$ ,  $\text{Ti}–\text{O}$  bond within the layer.

However,  $\text{FeTiO}_3$  is different from  $\text{MgTiO}_3$ . When  $\text{FeTiO}_3$  is heated to expand under high temperatures, the variation of the  $\text{Ti}–\text{Ti}$  bond length across the vacancy is approximately linear with the unit-cell volume. In contrast, the  $\text{Fe}–\text{Fe}$  bonds across vacancies are shortened rather than elongated when heated (Wechsler and Prewitt 1984). This anomaly implies that the essential cause of the anomalous thermal expansion of  $\text{FeTiO}_3$  is the  $\text{Fe}$  ion. The  $\text{Fe}–\text{O}$  bonds in  $\text{FeTiO}_3$  can be divided into longer and shorter ones; the shorter  $\text{Fe}–\text{O}$  bond is more difficult to elongate along its axes but easier to bend, and the elongation of the

longer  $\text{Fe}–\text{O}$  bond is twice that of the shorter one with the increase of temperature (Zhang et al. 2017). Analyzing the effect of the  $\text{FeO}_6$  layer and  $\text{TiO}_6$  layer on the thermal expansion separately for  $\text{FeTiO}_3$ , it can be seen that in  $\text{FeTiO}_3$ , the thermal expansion along the  $c$ -axis is smaller than that along the  $a$ -axis for the  $\text{FeO}_6$  layer, while the opposite is true for the  $\text{TiO}_6$  layer. Thus, we infer that the combined influences of  $\text{FeO}_6$  and  $\text{TiO}_6$  layers in  $\text{FeTiO}_3$  ultimately lead to its isotropic axial thermal expansivity. In addition, there are non-negligible magnetic properties between the  $\text{FeO}_6$  layers in  $\text{FeTiO}_3$  that weakly affect its thermal expansion behavior (Sansou et al. 2014).

$\text{Fe}$  is the transition metal element but  $\text{Mg}$  is not, thus  $\text{FeO}_6$  in the  $\text{FeTiO}_3$  is suitable for Ligand Field Theory (Dagroot et al. 1990) due to the d-layer electrons of transition metals, while  $\text{MgO}_6$  in the  $\text{MgTiO}_3$  is not applicable. Therefore,  $\text{FeO}_6$  has different deformation mechanisms from  $\text{MgO}_6$  when heated. A metal–metal interaction is allowed between the d orbitals extending their lobes through the face shared by the two octahedra, so the d orbital plane of  $\text{Fe}$  will extend its lobe through the shared surface of  $\text{FeO}_6$  (Chen et al. 2013). This allows the transfer of valence electrons along the  $\text{Fe}–\text{O}–\text{Ti}$  path, which makes the  $\text{Fe}^{2+}/\text{Ti}^{4+}$  part become a  $\text{Fe}^{3+}/\text{Ti}^{3+}$  structure. As a result, the structure of  $\text{FeTiO}_3$  is closer to the corundum structure (Radtke et al. 2006), which weakens the anisotropy of axial thermal expansibility and makes it closer to isotropic thermal expansivity. The intrinsic anharmonicity or electronic defects significantly affect the heat capacity and thermal expansion of  $\text{FeTiO}_3$ . In summary, the specificities of  $\text{Fe}$  ions and their relative bonds in  $\text{FeTiO}_3$  are the main reasons for the obvious difference in the axial thermal expansivity between  $\text{FeTiO}_3$  and  $\text{MgTiO}_3$ .

In this study, we obtained the thermal expansion coefficients of  $\text{FeTiO}_3$  and  $\text{MgTiO}_3$ . The thermal expansion coefficient is one of the essential thermal equations of state parameters to build the density model of  $\text{FeTiO}_3$  and  $\text{MgTiO}_3$  under the corresponding conditions of the lunar mantle. However, besides the thermal expansion coefficient, there still needs more thermal equations of state parameters, such as the bulk modulus and its pressure and temperature derivatives, which are jointly applied to the construction of the lunar mantle density model. In the future, we still need to carry out further research about the bulk modulus and its pressure and temperature derivatives of  $\text{FeTiO}_3$  and  $\text{MgTiO}_3$ , and then we can discuss the density models of  $\text{FeTiO}_3$  and  $\text{MgTiO}_3$ , the density model of lunar mantle and the kinetic process of lunar mantle overturning.

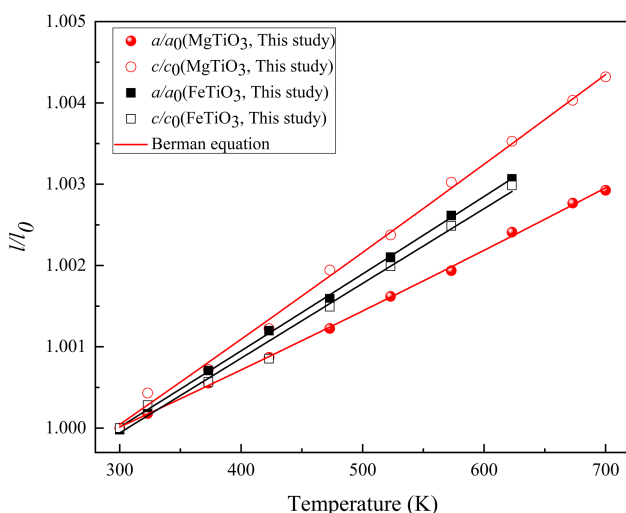


**Fig. 6** The axial expansion of  $\text{MgTiO}_3$  and  $\text{FeTiO}_3$  as a function of temperature. The error bars for the data points are not displayed because they are smaller than the symbols

## 5 Conclusion

- (1) In-situ high temperature experiments of  $\text{MgTiO}_3$  and  $\text{FeTiO}_3$  were conducted by synchrotron radiation ADXRD and DAC. No phase changes were observed for  $\text{MgTiO}_3$  and  $\text{FeTiO}_3$  within the temperature range (300–700 K).
- (2) By using Berman's equation to fit  $T$ - $V$  data,  $\alpha_{V0} = 2.55 (6) \times 10^{-5} \text{ K}^{-1}$  and  $\alpha_{V0} = 2.82 (10) \times 10^{-5} \text{ K}^{-1}$  of  $\text{MgTiO}_3$  and  $\text{FeTiO}_3$  are obtained. Meanwhile, we also obtained the axial thermal expansion coefficients for  $\text{MgTiO}_3$  and  $\text{FeTiO}_3$  along the  $a$ -axis ( $\alpha_{a0} = 0.74 (3) \times 10^{-5} \text{ K}^{-1}$  and  $\alpha_{a0} = 0.95 (5) \times 10^{-5} \text{ K}^{-1}$ , respectively) and  $c$ -axis ( $\alpha_{c0} = 1.08 (5) \times 10^{-5} \text{ K}^{-1}$  and  $\alpha_{c0} = 0.92 (12) \times 10^{-5} \text{ K}^{-1}$ , respectively).
- (3) The possible reasons for the difference between the volumetric thermal expansion coefficients of  $\text{FeTiO}_3$  and  $\text{MgTiO}_3$  are discussed. It is found that different compositions (Fe and Mg) at A site affect their volumetric thermal expansion coefficients.
- (4) The potential factors influencing the axial thermal expansion coefficients of  $\text{MgTiO}_3$  and  $\text{FeTiO}_3$  and the possible reasons for the different axial thermal expansion anisotropy between  $\text{MgTiO}_3$  and  $\text{FeTiO}_3$  were discussed. We infer that the specificity of Fe ions in  $\text{FeTiO}_3$  may be the main reason for the difference in the axial thermal expansivity between  $\text{FeTiO}_3$  and  $\text{MgTiO}_3$ .

**Acknowledgements** This project was supported by National Natural Science Foundation of China (U2032118 and 42172048), Guizhou Provincial Science and Technology Projects (QKHPTRC-YQK[2023]035 and QKHJC-ZK[2021]ZD042), Hundred Talents Program of the Chinese Academy of Sciences, and Guizhou Provincial 2020 and 2021 Science and Technology Subsidies (Nos. GZ2020SIG and GZ2021SIG). The high-temperature XRD experiments were conducted at the 4W2 of the Beijing Synchrotron Radiation Facility (BSRF).

**Author contributions** JS Methodology, Data analysis, Investigation, Writing-original draft, Writing-review & editing, Visualization. DF Supervision, Conceptualization, Review & editing. Shijie Huang: Methodology, Investigation. SZ Methodology, Investigation. MW Methodology, Investigation. WC Methodology, Investigation. WZ Investigation, Review & editing.

**Data availability** Data will be made available on request.

## Declarations

**Competing interest** The authors declare that they have no known competing financial interests or personal relationships that could have appeared to influence the work reported in this paper.

## References

- Alexander L, Snape JF, Crawford IA, Joy KH, Downes H (2014) Searching for nonlocal lithologies in the Apollo 12 regolith: a geochemical and petrological study of basaltic coarse fines from the Apollo lunar soil sample 12023,155. Meteorit Planet Sci 49:1288–1304. <https://doi.org/10.1111/maps.12319>
- Alexander L, Snape JF, Joy KH, Downes H, Crawford IA (2016) An analysis of Apollo lunar soil samples 12070, 889, 12030, 187, and 12070, 891: Basaltic diversity at the Apollo 12 landing site and implications for classification of small-sized lunar samples. Meteorit Planet Sci 51:1654–1677. <https://doi.org/10.1111/maps.12689>
- Anand M, Taylor LA, Neal CR, Snyder GA, Patchen A, Sano Y, Terada K (2003) Petrogenesis of lunar meteorite EET 96008. Geochim et Cosmochim Acta 67:3499–3518. [https://doi.org/10.1016/S0016-7037\(03\)00134-0](https://doi.org/10.1016/S0016-7037(03)00134-0)
- Angel RJ, Alvaro M, Gonzalez-Platas J (2014) EosFit7c and a Fortran module (library) for equation of state calculations. Zeitschrift für Kristallographie-Crystalline Materials 229:405–419. <https://doi.org/10.1515/zkri-2013-1711>
- Berman RG (1988) Internally-consistent thermodynamic data for minerals in the system  $\text{Na}_2\text{O}-\text{K}_2\text{O}-\text{CaO}-\text{MgO}-\text{FeO}-\text{Fe}_2\text{O}_3-\text{Al}_2\text{O}_3-\text{SiO}_2-\text{TiO}_2-\text{H}_2\text{O}-\text{CO}_2$ . J Petrol 29:445–522. <https://doi.org/10.1093/petrology/29.2.445>
- Chen S, Huang M, Lin P, Jeng H, Lee J, Haw S, Chen S, Lin H, Lu K, Chen D, Dou S, Wang X, Chen J (2013) Orbital structure of  $\text{FeTiO}_3$  ilmenite investigated with polarization-dependent X-ray absorption spectroscopy and band structure calculations. Appl Phys Lett 102:042107. <https://doi.org/10.1063/1.4789992>
- Culbertson CM, Flak AT, Yatskin M, Cheong PH-Y, Cann DP, Dolgos MR (2020) Neutron total scattering studies of group ii titanates ( $\text{ATiO}_3$ ,  $\text{A}^{2+} = \text{Mg, Ca, Sr, Ba}$ ). Sci Rep 10:3729. <https://doi.org/10.1038/s41598-020-60475-8>
- Degroot F, Grioni M, Fuggle JC, Thole B, Ghijssen J, Sawatzky G (1990) Ligand field effects in xas of 3d-transition metal compounds. In: Conference proceedings 25
- Donohue PH, Neal CR (2018) Textural and mineral chemical evidence for the cumulate origin and evolution of high-titanium basalt fragment 71597. Am Mineral: J Earth Planet Mater 103:284–297. <https://doi.org/10.2138/am-2018-6173>
- Fan D, Xu J, Liu J, Li Y, Xie H (2014) Thermal equation of state of natural stibnite up to 25.7 GPa and 533 K. High Temp High Pressures 43:351–359
- Fan D, Zhou W, Wei S, Liu Y, Ma M, Xie H (2010) A simple external resistance heating diamond anvil cell and its application for synchrotron radiation X-ray diffraction. Rev Sci Instr 81:053903. <https://doi.org/10.1063/1.3430069>
- Gonzalez-Platas J, Alvaro M, Nestola F, Angel R (2016) EosFit7-GUI: a new graphical user interface for equation of state calculations, analyses and teaching. J Appl Crystallogr 49:1377–1382. <https://doi.org/10.1107/S1600576716008050>
- Hammersley AP, Svensson O, Hanfland M, Fitch AN, Hausermann DM (1996) Two-dimensional detector software: from real detector to idealised image or two-theta scan. Int J High Pressure Res 14:235–248. <https://doi.org/10.1080/08957959608201408>
- Harrison RJ, Redfern SAT, Smith RI (2000) In-situ study of the R 3 to R 3 c phase transition in the ilmenite-hematite solid solution using time-of-flight neutron powder diffraction. Am Miner 85:194–205. <https://doi.org/10.2138/am-2000-0119>
- Heiken GH, Vaniman DT, French BM (1991) Lunar Sourcebook, a user's guide to the Moon. Cambridge University Press
- Henderson CMB, Neuhoff KS, Lennie AR (2009) Temperature dependence of rutile ( $\text{TiO}_2$ ) and geikielite ( $\text{MgTiO}_3$ ) structures

- determined using neutron powder diffraction. *Open Mineral J* 3:1–11. <https://doi.org/10.2174/1874456700903010001>
- Holland TJB, Redfern SAT (1997) Unit cell refinement from powder diffraction data: the use of regression diagnostics. *Mineral Mag* 61:65–77. <https://doi.org/10.1180/minmag.1997.061.404.07>
- Hu Z (2015) Moon: origin and evolution. Science Press
- Joy KH, Crawford IA, Anand M, Greenwood RC, Franchi IA, Russell SS (2008) The petrology and geochemistry of Miller Range 05035: a new lunar gabbroic meteorite. *Geochim et Cosmochim Acta* 72:3822–3844. <https://doi.org/10.1016/j.gca.2008.04.032>
- Klemme S, Günther D, Hametner K, Prowatke S, Zack T (2006) The partitioning of trace elements between ilmenite, ulvöspinel, armalcolite and silicate melts with implications for the early differentiation of the moon. *Chem Geol* 234:251–263. <https://doi.org/10.1016/j.chemgeo.2006.05.005>
- Li H, Zhang N, Liang Y, Wu B, Dygert NJ, Huang J, Parmentier EM (2019) Lunar cumulate mantle overturn: a model constrained by ilmenite rheology. *J Geophys Res: Planets* 124:1357–1378. <https://doi.org/10.1029/2018JE005905>
- Liforovich RP, Mitchell RH (2006) The pyrophanite–geikieelite solid-solution series: crystal structures of the  $Mn_{1-x}Mg_xTiO_3$  series ( $0 < x < 0.7$ ). *Can Mineral* 44:1099–1107. <https://doi.org/10.2113/gscanmin.44.5.1099>
- Lindsley DH (1991) Oxide minerals: petrologic and magnetic significance. *Rev Mineral Geochem*
- Linton JA, Fei Y, Navrotsky A (1999) The  $MgTiO_3$ – $FeTiO_3$  join at high pressure and temperature. *Am Miner* 84:1595–1603. <https://doi.org/10.2138/am-1999-1013>
- Radtke G, Lazar S, Botton GA (2006) High-resolution EELS investigation of the electronic structure of ilmenites. *Phys Rev B Condensed Matter Mater Phys* 74:155117. <https://doi.org/10.1103/PhysRevB.74.155117>
- Sanson A, Mathon O, Pasquarelli S (2014) Local vibrational dynamics of hematite ( $\alpha$ - $Fe_2O_3$ ) studied by extended x-ray absorption fine structure and molecular dynamics. *J Chem Phys* 140:224504. <https://doi.org/10.1063/1.4882282>
- Shannon RD (1976) Revised effective ionic radii and systematic studies of interatomic distances in halides and chalcogenides. *Acta Crystallogr Sect a: Cryst Phys Diffract Theor Gen Crystallogr* 32:751–767. <https://doi.org/10.1107/S0567739476001551>
- Shearer CK, Papike JJ, Galbreath KC, Shimizu N (1991) Exploring the lunar mantle with secondary ion mass spectrometry: a comparison of lunar picritic glass-beads from the apollo-14 and apollo-17 sites. *Earth Planet Sci Lett* 102:134–147. [https://doi.org/10.1016/0012-821X\(91\)90003-Z](https://doi.org/10.1016/0012-821X(91)90003-Z)
- Snape JF, Joy KH, Crawford IA, Alexander L (2014) Basaltic diversity at the Apollo 12 landing site: inferences from petrologic examinations of the soil sample 12003. *Meteorit Planet Sci* 49:842–871. <https://doi.org/10.1111/maps.12285>
- Tuval T, Rosen BA, Zabicky J, Kimmel G, Dilman H, Shneck RZ (2020) Thermal expansion of  $MgTiO_3$  made by sol-gel technique at temperature range 25–890 °C. *Crystals* 10:887. <https://doi.org/10.3390/crust10100887>
- Wechsler BA, Prewitt CT (1984) Crystal structure of ilmenite ( $FeTiO_3$ ) at high temperature and at high pressure. *Am Miner* 69:176–185
- Wechsler BA, Von Dreele RB (1989) Structure refinements of  $Mg_2TiO_4$ ,  $MgTiO_3$  and  $MgTi_2O_5$  by time-of-flight neutron powder diffraction. *Acta Crystallogr B* 45:542–549. <https://doi.org/10.1107/S010876818900786X>
- Wieczorek MA, Jolliff BL, Khan A, Pritchard ME, Weiss BP, Williams JG, Hood LL, Righter K, Neal CR, Shearer CK (2006) The constitution and structure of the lunar interior. *Rev Mineral Geochem* 60:221–364. <https://doi.org/10.2138/rmg.2006.60.3>
- Xu Y (2010) Mare basalts and lunar evolution. *Geochimica* 39:50–62. <https://doi.org/10.19700/j.0379-1726.2010.01.008>
- Yamanaka T, Komatsu Y, Nomori H (2007) Electron density distribution of  $FeTiO_3$  ilmenite under high pressure analyzed by MEM using single crystal diffraction intensities. *Phys Chem Miner* 34:307–318. <https://doi.org/10.1007/s00269-007-0149-7>
- Yamanaka T, Komatsu Y, Sugahara M, Nagai T (2005) Structure change of  $MgSiO_3$ ,  $MgGeO_3$ , and  $MgTiO_3$  ilmenites under compression. *Am Miner* 90:1301–1307. <https://doi.org/10.2138/am.2005.1621>
- Zhang N, Wang H, Wang G (2017) In-situ high temperature X-ray diffraction study of hematite. *Acta Petrologica Et Mineralogica* 36:89–95. <https://doi.org/10.3969/j.issn.1000-6524.2017.01.008>
- Zhao Y, de Vries J, van den Berg AP, Jacobs MHG, van Westrenen W (2019) The participation of ilmenite-bearing cumulates in lunar mantle overturn. *Earth Planet Sci Lett* 511:1–11. <https://doi.org/10.1016/j.epsl.2019.01.022>

Springer Nature or its licensor (e.g. a society or other partner) holds exclusive rights to this article under a publishing agreement with the author(s) or other rightsholder(s); author self-archiving of the accepted manuscript version of this article is solely governed by the terms of such publishing agreement and applicable law.